Al-Qadisiyah Journal of Pure Science

Volume 29 | Number 2 Article 7

12-20-2024

Motion analysis with a peristaltic flow temperature and concentration of Williamson fluid through an endoscopic hollow elastic channel

Walaa N. Al-Delfi
Department of Mathematics, College of Science, University of Al-Qadisiyah, Diwaneyah, Iraq, walaa.nk94@gmail.com

Dheia G. Salih Al-Khafajy
Department of Mathematics, College of Science, University of Al-Qadisiyah, Diwaneyah, Iraq, dr.dheia.g.salih@gmail.com

ORIGINAL STUDY

Motion Analysis With a Peristaltic Flow Temperature and Concentration of Williamson Fluid Through an Endoscopic Hollow Elastic Channel

Walaa N. Al-Delfi*, Dheia G. Al-khafajy

Department of Mathematics, College of Science, University of Al-Qadisiyah, Diwaneyah, Iraq

Abstract

This research aims to study and analyze the effect of temperature and concentration variation on the magneto-hydrodynamic peristaltic flow of Williamson fluid through a flexible porous channel with an endoscope in the centre of the channel. A magnetic field is created by the electrical conduction of a fluid flow channel. The coordinates used are cylindrical, assuming a long-wavelength "relative to the width of the channel to its length" the non-linear and non-homogeneous partial differential equations that govern the problem have been simplified, and by using dimensionless equations, we obtained the results of the problem through the "Mathematics 12" program these results analyzed.

Keywords: Williamson fluid, Magnetohydrodynamic(MHD), Peristaltic flow, Wall properties, An endoscope

1. Introduction

Peristalsis is a type of liquid carrier propelled along the length of a distensible cylinder containing liquids by a dynamic surge of constriction or extension. An area with lower compression is pumped to an area with higher compression [1]. Many smooth muscle cylinders appear to have this natural characteristic, including the gastrointestinal system, conceptive tract, fallopian tube, bile pipe, ureter, and throat. Peristalsis's mechanism has been used in the biomedical field and for commercial purposes [1,2].

Latham [3] coined the term "peristalsis" in 1966. Shapiro et al. [4]. have further investigated the phenomenon. The theoretical and experimental research studies have been discussed for various types of fluid flows in various channels of peristalsis [5]. Several scientists are also looking at how the magnetic field and the existence of permeability in the fluid flow channel interact [5–10]. Current research examines how temperature affects how liquids flow along a channel. Peristalsis is crucial for treating hyperthermia, arterial flow, cancer treatment, and other disorders where there are magnetic field effects present. In crucial applications like oil extraction from the ground and food absorption in the intestine, permeability plays a significant role in fluid transport. The majority of academics concur that a fluid's velocity increases as its temperature rises, however the difference in concentration has an uncertain effect on fluid velocity, which is what motivated us to submit this study.

1.1. Mathematical formulation

Consider the Williamson fluid flowing magnetohydrodynamically peristaltically through a flexible porous channel with an endoscope positioned at the channel's cylindrical center (see Fig. 1).

It is defined as the geometry of the wall surface:

$$\left.\begin{aligned} &\bar{r}=\overline{r_1}=a_1 && \text{Inner wall} \\ &\bar{r}=\overline{r_2}(\bar{z},\bar{t})=a_2+b\,Sin\left(\frac{2\pi}{\mathcal{L}}(\bar{z}-s\bar{t})\right) && \text{Outer wall} \end{aligned}\right\} \tag{1}$$

Received 18 February 2022; accepted 20 June 2022.
Available online 18 April 2025

* Corresponding author.
E-mail addresses: walaa.nk94@gmail.com (W.N. Al-Delfi), dr.dheia.g.salih@gmail.com, dheia.salih@qu.edu.iq (D.G. Al-khafajy).

https://doi.org/10.29350/2411-3514.1284

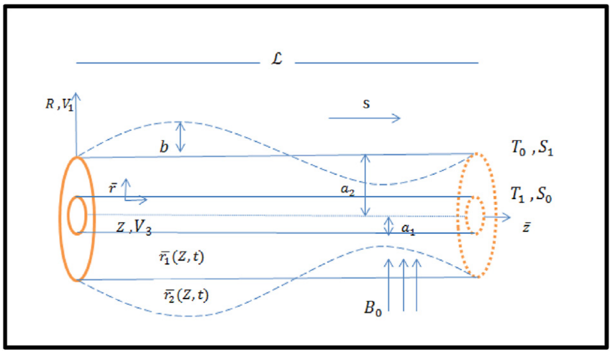

Fig. 1. The problem Geometry.

Such a_2 is currently an undisturbed channel's average radius, b was the peristaltic wave's amplitude, $\mathcal{L}$ that wavelength, s was the speed of wave propagation, and $\bar{t}$ is the time.

2. Basic equations

The fundamental equations regulating the incompressible non-Newtonian fluid known as the Williamson fluid are supplied.

The continuity equation is given

$$\nabla \overline{V} = 0 \tag{2}$$

The equation of momentum

$$\rho(\overline{V}\,.\,\overline{\nabla}\,)\overline{V} = \overline{\nabla}\left(-\overline{p}\,\overline{I} + \overline{\tau}\right) + \mu_p \overline{j} \times \overline{B} + \rho g \beta_1 (T - T_0) + \rho g \beta_1 (S - S_0) - \frac{\mu}{K^*}\overline{V_1} \tag{3}$$

The equation of temperature it's given by:

$$T_u.\rho(\overline{V}.\nabla)T = T_m.\nabla^2 T - \nabla.Q_r - Q(T - T_0) \tag{4}$$

The equation of concentration is given:

$$(\overline{V}\,.\nabla)S = G_n \nabla^2 S + \frac{G_n T_e}{T_n}\nabla^2 T \tag{5}$$

Where $\nabla^2 = \frac{1}{r}\frac{\partial}{\partial r}\left(r\frac{\partial}{\partial r}\right)$ (Laplace operator), $\overline{V}$ a velocity field, ρ is a density, and ∇V is the fluid velocity gradient, μ_p is the magnetic permeability; also μ is the dynamic viscosity, $\overline{I}$ is induced current, $\overline{B} = (0, B_0, 0)$ is the magnetic field, and $\overline{J}$ represents the Cauchy stress tensor, T is the temperature, S is the concentration of the fluid, T_u is the specific heat capacity at constant pressure, T_m is the thermal conductivity, Q_r is the radiation heat flux G_n is the coefficient of mass diffusivity, T_n is a fluid's average temperature, K_T is the thermal diffusion ratio, K^* is the permeability and Q heat generation.

The following are the constitutive equations for an incompressible Williamson fluid;

$$\overline{\tau} = \left[\mu_\infty + (\mu_0 + \mu_\infty)(1 - \Gamma\overline{\dot{\gamma}})^{-1}\right]\overline{\dot{\gamma}} \tag{6}$$

Where τ the additional stress tensor, μ_∞ is the endless shear viscosity, μ_0 the viscosity at zero shear rate, Γ time is a constant and $\dot{\gamma}$ is shear strain is described in the coordinates of cylindrical (r, θ, z) as follows.

3. Method of solution

The public and private two-frame coordinate transformations are given by;

$\bar{r} = \overline{R}$, $\overline{v_1} = \overline{V_1}$, $\overline{v_3} = \overline{V_3} - s$, $\bar{z} = \overline{Z} - s\bar{t}$

where $(\overline{v_1}, \overline{v_3})$ and $(\overline{V_1}, \overline{V_3})$ are velocity components in the moving and static frames, respectively. By using these transforms, The problem's equations are:

$$\frac{\partial \overline{v_1}}{\partial \bar{r}} + \frac{\overline{v_1}}{\bar{r}} + \frac{\partial(\overline{v_3} + s)}{\partial \bar{z}} = 0 \tag{7}$$

$$\rho\left(\frac{\partial \overline{v_1}}{\partial \bar{t}} + \overline{v_1}\frac{\partial \overline{v_1}}{\partial \bar{r}} + (\overline{v_3} + s)\frac{\partial \overline{v_1}}{\partial \bar{z}}\right) = -\frac{\partial \bar{p}}{\partial \bar{r}} + \frac{1}{\bar{r}}\frac{\partial}{\partial \bar{r}}(\bar{r}\overline{\tau}_{\bar{r}\bar{r}}) + \frac{\partial}{\partial \bar{z}}(\overline{\tau}_{\bar{r}\bar{z}}) - \frac{\overline{\tau}_{\bar{\vartheta}\bar{\vartheta}}}{\bar{r}} - \frac{\mu}{K^*}\overline{v_1} - \sigma B_0^2 \overline{v_1} \tag{8}$$

$$\rho\left(\frac{\partial(\overline{v_3} + s)}{\partial \bar{t}} + \overline{v_1}\frac{\partial(\overline{v_3} + s)}{\partial \overline{R}} + (\overline{v_3} + s)\frac{\partial(\overline{v_3} + s)}{\partial \bar{z}}\right) = -\frac{\partial \bar{p}}{\partial \bar{z}} + \frac{1}{\bar{r}}\frac{\partial}{\partial \bar{r}}(\bar{r}\overline{\tau}_{\bar{r}\bar{z}}) + \frac{\partial}{\partial \bar{z}}(\overline{\tau}_{\bar{z}\bar{z}}) + \rho g \beta_1 (T - T_0) + \rho g \beta_2 (S - S_0) - \frac{\mu}{K^*}(\overline{v_3} + s) - \sigma B_0^2(\overline{v_3} + s) \tag{9}$$

$$\frac{\partial T}{\partial \bar{t}} + \overline{v_1}\frac{\partial T}{\partial \overline{R}} + (\overline{v_3} + s)\frac{\partial T}{\partial \overline{Z}} = \frac{T_m}{T_u \rho}\left(\frac{\partial^2 T}{\partial \bar{r}^2} + \frac{1}{\bar{r}}\frac{\partial T}{\partial \bar{r}} + \frac{\partial^2 T}{\partial \bar{z}^2}\right) + \frac{16\sigma_0 T_2^E}{3k_0 T_u\,\rho}\frac{1}{\bar{r}}\frac{\partial}{\partial \bar{r}}\left(\frac{\partial T}{\partial \bar{r}}\right) - \frac{q}{T_u\,\rho}(T - T_0) \tag{10}$$

$$\frac{\partial S}{\partial \bar{t}} + \overline{v_1}\frac{\partial S}{\partial \bar{r}} + (\overline{v_3} + s)\frac{\partial S}{\partial \bar{z}} = G_n\left(\frac{\partial^2 S}{\partial \bar{r}^2} + \frac{1}{\bar{r}}\frac{\partial S}{\partial \bar{r}} + \frac{\partial^2 S}{\partial \bar{z}^2}\right) + \frac{G_n T_e}{T_n}\left(\frac{\partial^2 T}{\partial \bar{r}^2} + \frac{1}{\bar{r}}\frac{\partial T}{\partial \bar{r}} + \frac{\partial^2 T}{\partial \bar{r}^2}\right) \tag{11}$$

$$\overline{\tau}_{\bar{r}\,\bar{r}} = 2(\mu_0 + (\mu_0 - \mu_0)\Gamma\dot{\gamma})\left(2\frac{\partial \overline{v_1}}{\partial \bar{r}}\right)$$

$$\overline{\tau}_{\bar{r}\,z} = (\mu_0 + (\mu_0 - \mu_\infty)\Gamma\dot{\gamma})\left(\frac{\partial \overline{V_1}}{\partial \bar{z}} + \frac{\partial(\overline{v_3} + s)}{\partial \bar{r}}\right)$$

$$\overline{\tau}_{\bar{z}\bar{z}} = 2\mu_\circ(1 + \Gamma|\overline{\dot{\gamma}}|)\left(2\frac{\partial(\overline{v_3} + s)}{\partial \bar{z}}\right)$$

The corresponding boundary conditions

$$\overline{v_3} = -1, \overline{v_1} = 0, T = T_0, S = S_1, at\, \bar{r} = \overline{r_1} = a_1$$

$$\overline{v_3} = -1, \overline{v_1} = 0, T = T_1, S = S_0, at\, \bar{r} = \overline{r_2}(\bar{z}, \bar{t}) = a_2 + b\, Sin\left(\frac{2\pi}{\mathcal{L}}(\bar{z} - s\bar{t})\right)$$

It has been discovered the formula controlling the properties of flexible wall channel at $\bar{r} = \overline{r_2}$;

$$L^*(\overline{r_2}) = \bar{p} - \bar{p}_0 = A\frac{\partial^4}{\partial \overline{Z}^4} - B\frac{\partial^2}{\partial \overline{Z}^2} + C\frac{\partial^2}{\partial \bar{t}^2} + D\frac{\partial}{\partial \bar{t}} + E_L \qquad (12)$$

where A is a wall's flexural stiffness, B is a longitudinal tension per unit width, C is a mass per unit area, D is a viscous damping coefficient and E_L is the stiffness of a spring.

We can introduce the following dimensionless transformations to reduce the complexity of the motion's governing equations:

$$\left.\begin{array}{l} v_1 = \frac{\overline{v_1} L}{a_2 s}, v_3 = \frac{\overline{v_3}}{s}, r = \frac{\bar{r}}{a_2}, z = \frac{\bar{z}}{L}, \tau = \frac{a_2 \bar{\tau}}{\mu\, s}, \delta = \frac{a_2}{L}, t = \frac{s\bar{t}}{L}, p = \frac{a_2^2 \bar{p}}{\mu s L}, \dot{\gamma} = \frac{a_2 \bar{\dot{\gamma}}}{s}, \varnothing = \frac{b}{a_2}, \\ \mathcal{H} = \frac{T - T_0}{T_1 - T_0}, S = \frac{s - s_0}{s_1 - s_0}, \Omega = \frac{q a_2^2}{\mu T_p}, W_e = \frac{\Gamma s}{a_2}, r_1 = \frac{\bar{r}_1}{a_2} = \varepsilon < 1, r_2 = \frac{\bar{r}_2}{a_2} = 1 + \varnothing \sin(2\pi \bar{z}) \end{array}\right\} \qquad (13)$$

where "$\varnothing$ amplitude ratio, Re Reynolds number, δ dimensionless wave number, W_e Weissenberg number", also "$Re = \frac{\rho s a_2}{\mu}$ Reynolds number, $Pr = \frac{\mu T_m}{T_u}$ the Prandtl number, $D_a = \frac{k^*}{a_2^2}$ Darcy number, $Sc = \frac{\mu}{\rho G_n}$ Schmidt number, $Sr = \frac{\rho g G_n T_e (T_1 - T_0)}{\mu T_m (s_1 - s_0)}$ Sort number, $Gr = \frac{\rho g \beta_1 a_2^2 (T_1 - T_0)}{\mu s}$ thermal Grashof number, $Rn = \frac{k_0 T_m \mu}{4 T_{2\sigma_0}^E}$ thermal radiation parameter, $M^2 = \frac{\sigma a_2^2 B_0^2}{\mu}$ magnetic parameter, $Gc = \frac{\rho g \beta_2 a_2^2 (s_1 - s_0)}{\mu s}$ Solutal Grashof.

Introducing non-dimensional analysis (13) for equations (7)−(12) and then dropping over-bars, the above boundary conditions and governing equations can be rewritten as follows;

$$\left(\frac{S}{L}\right)\left(\frac{\partial v_1}{\partial r} + \frac{v_1}{r} + \frac{\partial v_3}{\partial z}\right) = 0 \qquad (14)$$

$$\mathrm{Re}\delta^3\left(\frac{\partial v_1}{\partial t} + v_1\frac{\partial v_1}{\partial r} + (v_3 + 1)\frac{\partial v_1}{\partial z}\right) = \frac{-\partial p}{\partial r} + \delta\frac{1}{r}\frac{\partial}{\partial r} r\tau_{rr} + \delta^2\frac{\partial}{\partial z}(\tau_{rz}) - \delta\frac{\tau_{\theta\theta}}{r} - \frac{\delta^2}{D_a}v_1 - \delta^2 M^2 v_1 \qquad (15)$$

$$\mathrm{Re}\delta\left(\frac{\partial v_3}{\partial t} + v_1\frac{\partial v_3}{\partial r} + (v_3 + 1)\frac{\partial v_3}{\partial z}\right) = \frac{-\partial p}{\partial z} + \frac{1}{r}\tau_{rz} + \frac{\partial}{\partial r}\tau_{rz} + \delta\frac{\partial}{\partial z}\tau_{zz} - \left(M^2 + \frac{1}{D_a}\right)v_3 - \left(M^2 + \frac{1}{D_a}\right) + Gr\mathcal{H} + GcS \qquad (16)$$

$$Re\,\delta\left(\frac{\partial T}{\partial t} + v_1\frac{\partial \mathcal{H}}{\partial r} + (v_3 + 1)\frac{\partial \mathcal{H}}{\partial z}\right) = \frac{1}{Pr}\left(\frac{\partial^2 \mathcal{H}}{\partial r^2} + \frac{1}{r}\frac{\partial \mathcal{H}}{\partial r} + \delta^2\frac{\partial^2 \mathcal{H}}{\partial z^2}\right) + \frac{4}{3Rn}\frac{1}{r}\frac{\partial}{\partial r}\left(r\frac{\partial \mathcal{H}}{\partial r}\right) - \Omega\mathcal{H} \qquad (17)$$

$$Re\,\delta\left(\frac{\partial S}{\partial t} + v_1\frac{\partial S}{\partial r} + (v_3 + 1)\frac{\partial S}{\partial z}\right) = \frac{1}{SC}\left(\frac{\partial^2 S}{\partial r^2} + \frac{1}{r}\frac{\partial S}{\partial r} + \delta^2\frac{\partial^2 S}{\partial z^2}\right) + Sr\left(\frac{\partial^2 \mathcal{H}}{\partial r^2} + \frac{1}{r}\frac{\partial \mathcal{H}}{\partial r} + \delta^2\frac{\partial^2 \mathcal{H}}{\partial z^2}\right) \qquad (18)$$

The relevant boundary conditions for the dimensionless variables in the wave frame are as follows:

$$\left.\begin{array}{l} v_3 = -1, v_1 = 0, \mathcal{H} = 0, S = 1, at\, r = r_1 = \varepsilon \\ v_3 = -1, v_1 = 0, \mathcal{H} = 1, S = 0, at\, r = r_2 \\ = 1 + \varnothing.Sin(2\pi(z - t)) \end{array}\right\} \qquad (19)$$

The pressure at the fluid−wall interface must be the same as the pressure acting on the fluid, according to stress continuity. The momentum equation is used to calculate the dynamic boundary conditions at the elastic walls.

$$k_1\frac{\partial^5(r_2)}{\partial z^5} - k_2\frac{\partial^3(r_2)}{\partial z^3} + k_3\frac{\partial^3(r_2)}{\partial z \partial t^2} + k_4\frac{\partial^2(r_2)}{\partial z \partial t} + k_5\frac{\partial(r_2)}{\partial z} = \frac{1}{r}\frac{\partial}{\partial r}(r\tau_{rz}) - \left(M^2 + \frac{1}{D_a}\right)v_3 - \left(M^2 + \frac{1}{D_a}\right) + Gr\mathcal{H} + GcS \qquad (20)$$

where $k_1 = \frac{Aa_2^3}{\mu s L^5}$ is a wall's flexural stiffness, $k_2 = -\frac{Ba_2^3}{\mu s L^3}$ is a longitudinal tension per unit width, $k_3 = \frac{Csa_2^3}{\mu L^3}$ is a mass per unit area, $k_4 = \frac{Da_2^3}{\mu L^2}$ is a viscous damping coefficient, and $k_5 = \frac{E_L a_2^3}{\mu s L}$ is the stiffness of a spring.

We shall restrict our analysis to the premise of a tiny dimensionless wave number because it seems impossible to address the problem in its generalized form δ≪1. To put it another way, we discovered the approximate long wavelength. This assumption leads to Equations (14)–(20):

$$\frac{\partial v_1}{\partial r} + \frac{v_1}{r} + \frac{\partial v_3}{\partial z} = 0 \tag{21}$$

$$\frac{\partial p}{\partial r} = 0 \tag{22}$$

$$\frac{\partial p}{\partial z} = \frac{1}{r}\frac{\partial}{\partial r}(r\tau_{rz}) - \left(M^2 + \frac{1}{D_a}\right)v_3 - \left(M^2 + \frac{1}{D_a}\right) + Gr\mathcal{H} + GcS \tag{23}$$

$$\left(\frac{1}{Pr} + \frac{4}{3Rn}\right)\frac{1}{r}\frac{\partial}{\partial r}\left(r\frac{\partial \mathcal{H}}{\partial r}\right) - \Omega\mathcal{H} = 0 \tag{24}$$

$$\frac{1}{Sc}\left(\frac{\partial^2 S}{\partial r^2} + \frac{1}{r}\frac{\partial S}{\partial r}\right) = -Sr\left(\frac{\partial^2 \mathcal{H}}{\partial r^2} + \frac{1}{r}\frac{\partial \mathcal{H}}{\partial r}\right) \tag{25}$$

$$k_1\frac{\partial^5(r_2)}{\partial z^5} - k_2\frac{\partial^3(r_2)}{\partial z^3} + k_3\frac{\partial^3(r_2)}{\partial z\partial t^2} + k_4\frac{\partial^2(r_2)}{\partial z\partial t} + k_5\frac{\partial(r_2)}{\partial z} = \frac{1}{r}\frac{\partial}{\partial r}(r\tau_{rz}) - \left(M^2 + \frac{1}{D_a}\right)v_3 - \left(M^2 + \frac{1}{D_a}\right) + Gr\mathcal{H} + GcS \tag{26}$$

where

$$\tau_{rr} = \tau_{zz} = 0 \; and \; \tau_{rz} = \left(\frac{\partial v_3}{\partial r} + We\left(\frac{\partial v_3}{\partial r}\right)^2\right) \tag{27}$$

Replacing τ_{rz} from equation (27) in equation (20), we have:

$$k_1\frac{\partial^5(r_2)}{\partial z^5} - k_2\frac{\partial^3(r_2)}{\partial z^3} + k_3\frac{\partial^3(r_2)}{\partial z\partial t^2} + k_4\frac{\partial^2(r_2)}{\partial z\partial t} + k_5\frac{\partial(r_2)}{\partial z} = \frac{1}{r}\frac{\partial}{\partial r}\left(r\left(\frac{\partial v_3}{\partial r} + We\left(\frac{\partial v_3}{\partial r}\right)^2\right)\right) - \left(M^2 + \frac{1}{D_a}\right)v_3 - \left(M^2 + \frac{1}{D_a}\right) + Gr\mathcal{H} + GcS \tag{28}$$

4. Temperature and concentration equation solutions

Rewrite the temperature equation (24) as follow:

$$\frac{\partial^2 \mathcal{H}}{\partial r^2} + \frac{1}{r}\frac{\partial \mathcal{H}}{\partial r} = -A\mathcal{H} \tag{29}$$

where $A = \frac{-\Omega}{\left(\frac{1}{Pr} + \frac{4}{3Rn}\right)}$, with the boundary condition $\mathcal{H}(r_1) = 0, \mathcal{H}(r_1) = 1$. So that the solution are

$$\mathcal{H} = J_0[0, \sqrt{A}r]c_1 + Y_0[0, \sqrt{A}r]c_2 \tag{30}$$

where $c_1 = \frac{Y_0[0,\sqrt{A}\epsilon]}{-J_0[0,\sqrt{A}\,\epsilon]Y_0[0,\sqrt{A}\,h] + J_0[0,\sqrt{A}\,h]Y_0[0,\sqrt{A}\in]}$ and $c_2 = \frac{J_0[0,\sqrt{A}\epsilon]}{J_0[0,\sqrt{A}\,\epsilon]Y_0[0,\sqrt{A}\,h] - J_0[0,\sqrt{A}\,h]Y_0[0,\sqrt{A}\in]}$

The concentration equation (28), as follows:

$$\frac{\partial^2 S}{\partial r^2} + \frac{1}{r}\frac{\partial S}{\partial r} = -B\mathcal{H}$$

where $B = \frac{\Omega * S_c S_r}{\left(\frac{1}{Pr} + \frac{4}{3Rn}\right)}$, with the boundary condition $S(r_1) = 1, S(r_1) = 0$. So that the solution are

$$S = \left(\frac{BJ_0[0,\sqrt{A}\epsilon]Y_0[0,\sqrt{A}r]}{A(J_0[0,\sqrt{A}\epsilon]Y_0[0,\sqrt{A}h] - J_0[0,\sqrt{A}h]Y_0[0,\sqrt{A}\epsilon])} - \frac{B(-1 + J_0[0,\sqrt{A}r])Y_0[0,\sqrt{A}\epsilon]}{A(J_0[0,\sqrt{A}\epsilon]Y_0[0,\sqrt{A}h] - J_0[0,\sqrt{A}h]Y_0[0,\sqrt{A}\in])}\right) + c_4 + c_3\,\mathrm{Log}[r]$$

where $c_3 = -\frac{A+B}{A(\mathrm{Log}[h] - \mathrm{Log}[\epsilon])}$, and

$$c_4 = -\frac{\left(\begin{array}{l} -A\,J_0\left[0,\sqrt{A}\,\epsilon\right]Y_0\left[0,\sqrt{A}\,h\right]Log[h] + BY_0\left[0,\sqrt{A}\,\epsilon\right]Log[h] + A\,J_0\left[0,\sqrt{A}\,h\right]Y_0\left[0,\sqrt{A}\,\epsilon\right]Log[h] - \\ B\,J_0\left[0,\sqrt{A}\,\epsilon\right]Y_0\left[0,\sqrt{A}\,h\right]Log[\in] - B\,Y_0\left[0,\sqrt{A}\,\epsilon\right]Log[\in] + B\,J_0\left[0,\sqrt{A}\,h\right]Y_0\left[0,\sqrt{A}\,h\right]Log[\in] \end{array}\right)}{A\left(J_0[0,\sqrt{A}\,\epsilon]Y_0[0,\sqrt{A}\,h] - J_0[0,\sqrt{A}\,h]Y_0[0,\sqrt{A}\in]\right)(Log[h] - Log[\in])}$$

The corresponding stream function is $v_1 = -\frac{1}{r}\frac{\partial\psi}{\partial z}$ and $v_3 = \frac{1}{r}\frac{\partial\psi}{\partial r}$.

5. Perturbation method solution

The momentum and stream functions are found in this section. Due to the nonlinear of equation (28), an accurate solution might not be feasible. As a result, we use a of the regular perturbation method to locate the answer of *We* "Weissenberg number" for a second order. For perturbation solution, we expand as

$$v_3 = v_{03} + We\,v_{13} + O\left(We^2\right) \tag{31}$$

Substituting equation (31) into equation (28) with boundary conditions, then equating the like powers of *We*, we obtain

5.1. Zero-order

$$\mathrm{L} = \frac{\partial^2 \mathrm{v}_{03}}{\partial \mathrm{r}^2} + \frac{1}{r}\frac{\partial \mathrm{v}_{03}}{\partial \mathrm{r}} - \left(M^2 + \frac{1}{D_a}\right)v_{03} \tag{32}$$

With boundary condition
$v_{03} = -1, at \quad r = r_1 = \varepsilon$
$and \;\; r = r_2 = 1 + \varnothing.Sin(2\pi(z-t))$ where

$$L = k_1\frac{\partial^5(r_2)}{\partial z^5} - k_2\frac{\partial^3(r_2)}{\partial z^3} + k_3\frac{\partial^3(r_2)}{\partial z\partial t^2} + k_4\frac{\partial^2(r_2)}{\partial z\partial t} + k_5\frac{\partial(r_2)}{\partial z} + \left(M^2 + \frac{1}{D_a}\right) - Gr\mathcal{H} - GcS$$

5.2. First order

$$\frac{1}{r}\frac{\partial^2 \mathrm{v}_{13}}{\partial \mathrm{r}^2} + \frac{1}{r}\frac{\partial \mathrm{v}_{13}}{\partial \mathrm{r}} - \frac{1}{r}\left(M^2 + \frac{1}{D_a}\right)v_{13} = -2\frac{1}{r}\left(\frac{\partial \mathrm{v}_{03}}{\partial \mathrm{r}}\right) \times \left(\frac{\partial^2 \mathrm{v}_{03}}{\partial \mathrm{r}^2}\right) - \left(\frac{\partial \mathrm{v}_{03}}{\partial \mathrm{r}}\right)^2 \tag{33}$$

With boundary condition

$v_{13} = 0, at \quad r = r_1 = \varepsilon$ and $r = r_2 = 1 + \varnothing.Sin(2\pi(z-t))$

6. Discussion and the quantitative findings

In this paragraph, we go over the conclusions we came to after utilizing the perturbation method to solve the problem's equations and MATHEMATICA to visualize the conclusions. This section is broken up into three sections: The first discusses the effect of heat and concentration on the movement of liquid; the second explains how parameters affect how fluid moves through the flow channel; and the third describes how parameters affect the fluid flow routes.

6.1. Temperature and concentration distribution

Figs. (2)-(6) illustrates parameter results Ω, ε, $\varnothing$, R_n, and Pr on temperature distribution function $\mathcal{H}$ and concentration distribution function S Where we

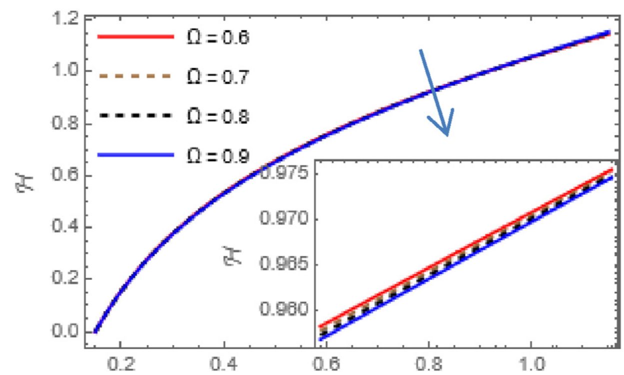

Fig. 2. Temperature variations $\mathcal{H}$ vs. r at $\epsilon = 0.3$, $\varnothing = 0.3$, $Rn = 0.1$, $Pr = 2$, $z = 0.1$.

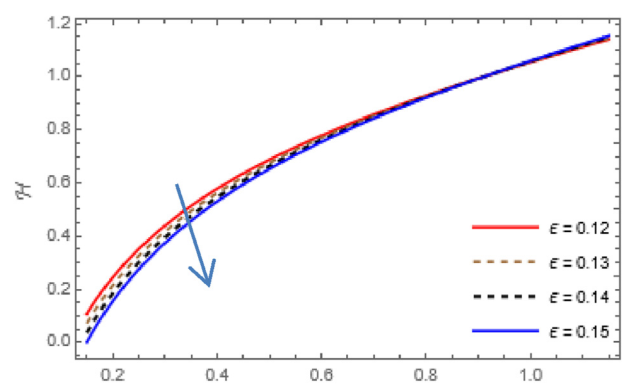

Fig. 3. Temperature variations $\mathcal{H}$ vs. r at $\Omega = 0.9$, $\varnothing = 0.3$, $Rn = 0.1$, $Pr = 2$, $z = 0.1$.

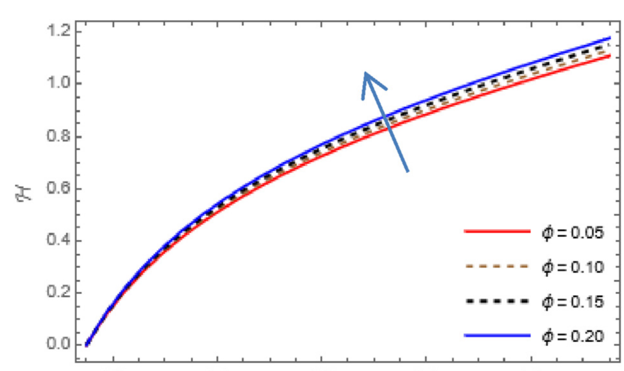

Fig. 4. Temperature variations $\mathcal{H}$ vs. r at $\Omega = 0.9$, $\epsilon = 0.3$, $Rn = 0.1$, $Pr = 2$, $z = 0.1$.

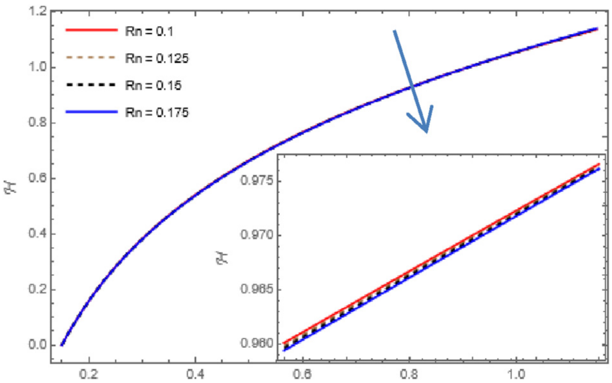

Fig. 5. Temperature variations $\mathcal{H}$ vs. r at $\Omega = 0.9$, $\varnothing = 0.3$, $\epsilon = 0.3$, $Pr = 2$, $z = 0.1$.

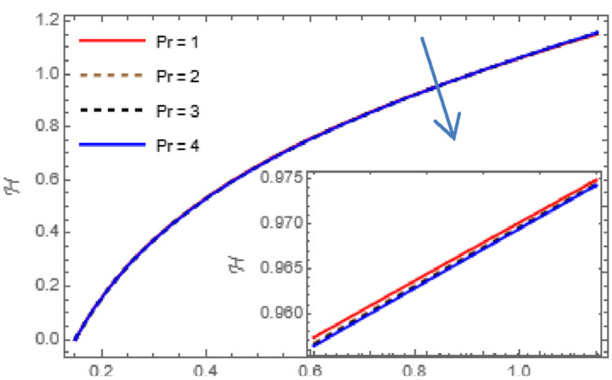

Fig. 6. Temperature variations $\mathcal{H}$ vs. r at $\Omega = 0.9$, $\epsilon = 0.3$, $Rn = 0.1$, $\varnothing = 0.3$, $z = 0.1$.

notice that $\mathcal{H}$ decreases against the parameters ε, R_n, Ω and Pr, respectively, while $\mathcal{H}$ increases with increasing of $\varnothing$.

Figs. (7-13) show that the effect of all parameters Ω, ε, $\varnothing$, Rn, Sr, Sc, and Pr on concentration function is direct.

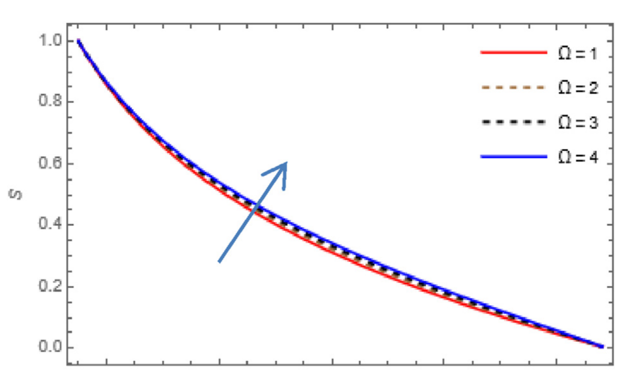

Fig. 7. Concentration variation S vs. r at $\varepsilon = 0.2$, $\varnothing = 0.2$, $Sr = 0.6$, $Sc = 0.5$, $Rn = 0.5$, $Pr = 2$, $z = 0.1$.

6.2. Velocity distribution

Figs. (14-30) illustrate the effect of parameters W_e, $\varnothing$, L_1, L_2, L_3, L_4, L_5, ε, Ω, $\varnothing$, R_n, Sr, Sc, Pr, M, D_a, Gr,

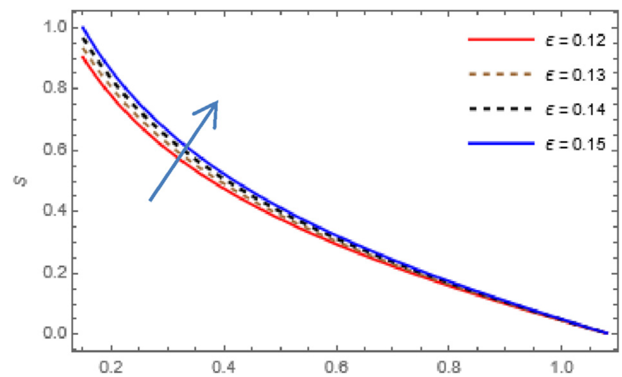

Fig. 8. Concentration variation S vs. r at $\Omega = 0.2$, $\varnothing = 0.2$, $Sr = 0.6$, $Sc = 0.5$, $Rn = 0.5$, $Pr = 2$, $z = 0.1$.

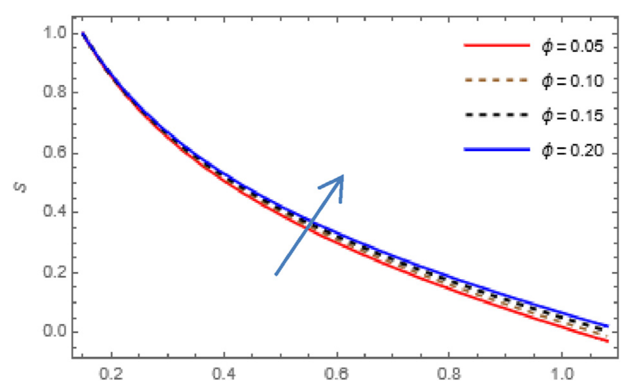

Fig. 9. Concentration variation S vs. r at $\Omega = 0.2$, $\varepsilon = 0.2$, $Sr = 0.6$, $Sc = 0.5$, $Rn = 0.5$, $Pr = 2$, $z = 0.1$.

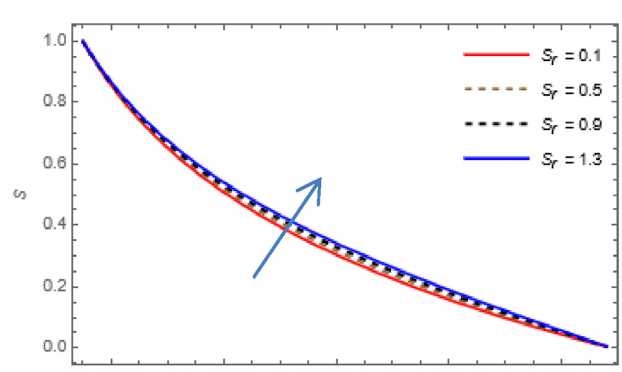

Fig. 10. Concentration variation S vs. r at $\Omega = 0.2$, $\varepsilon = 0.2$, $\varnothing = 0.2$, $Sc = 0.5$, $Rn = 0.5$, $Pr = 2$, $z = 0.1$.

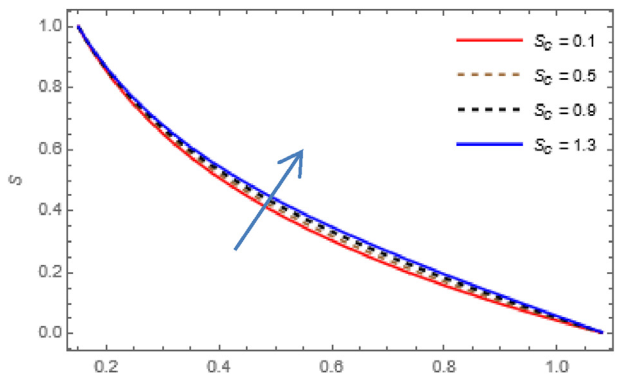

Fig. 11. Concentration variation S vs. r at $\Omega = 0.2$, $\varepsilon = 0.2$, $\varnothing = 0.2$, $Sr = 0.6$, $Rn = 0.5$ $Pr = 2$, $z = 0.1$.

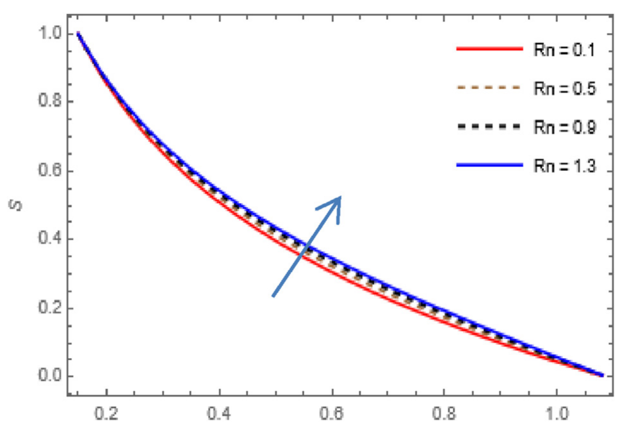

Fig. 12. Concentration variation S vs. r at $\Omega = 0.2$, $\varepsilon = 0.2$, $\varnothing = 0.2$, $Sr = 0.6$, $Sc = 0.5$, $Pr = 2$, $z = 0.1$.

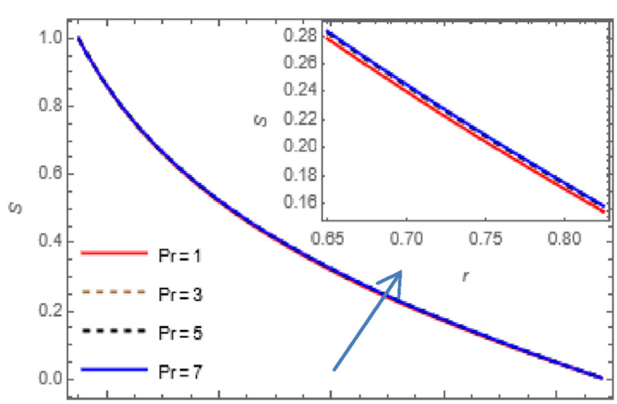

Fig. 13. Concentration variation S vs. r at $\Omega = 0.2$, $\varepsilon = 0.2$, $\varnothing = 0.2$, $Sr = 0.6$, $Sc = 0.5$, $Rn = 0.5$, $z = 0.1$.

and Gc on the distribution of velocity v_3 vs r, respectively. Where we notice that v_3 we notice the decreases in the velocity when increasing ε, L_3 , L_4 and M. while v_3 we notice the effect of parameters; it is the velocity increase when increasing $\varnothing$, W_e, L_5, L_2, L_1, R_n, Sr, Sc, Pr, Gc, D_a, Gr, and Ω .

6.3. Phenomena trapping

Due to the peristaltic motion of the flow channel wall impacting the fluid flow within the channel, the closed streamlines of the bolus are created; in this section, we will discuss the effect of parameters W_e, $\varnothing$, L_1, L_2, L_3, L_4, L_5, ε, Ω, $\varnothing$, Rn, Sr, Sc, Pr, M, D_a, Gr, and Gc. Fig. (31), We notice the growth of a gap inside the channel, which continues to grow, leading to a decrease in the number of bracelets in the channel when the parameter is increased ε. In Fig. (32), We note that the stuck bolus expands and grows steadily in the centre of the channel and expands to the outer walls (elastic wall) with increasing parameters $\varnothing$. Fig. (33), We note that the trapped bolus increases and grows steadily in the centre of the channel and expands to the outer walls (elastic wall) with increasing parameter W_e.In Fig. (34), We note that the stuck bolus expands and grows steadily in the centre of the channel and expands to the outer walls (elastic wall) with increasing parameter L_5.In Fig. (35), We note the effect of the parameter L_3 is the contraction of the trapped bolus when the parameter is increased L_3. Fig. (36), We note that the stuck bolus expands and grows steadily in the centre of the channel and expands to the outer walls (elastic wall) with increasing parameter L_1. In Fig. (37), We note that the trapped bolus increases and grows steadily in the centre of the channel and expands to the outer walls (elastic wall) with increasing parameter L_2. In Fig. (38), We note that the stuck bolus expands and grows steadily in the centre of the channel and expands to the outer walls (elastic wall) with increasing parameter D_a. In Fig. (39), We note that the stuck bolus expands and grows steadily in the centre of the channel and expands to the outer walls (elastic wall) with increasing parameter Gr. In Fig. (40), We note the effect of the parameter M is the contraction of the trapped bolus when the parameter is increased M While we find that the parameters L_4, Ω, R_n, Sr, Sc, Pr, and Gc have a very weak effect.

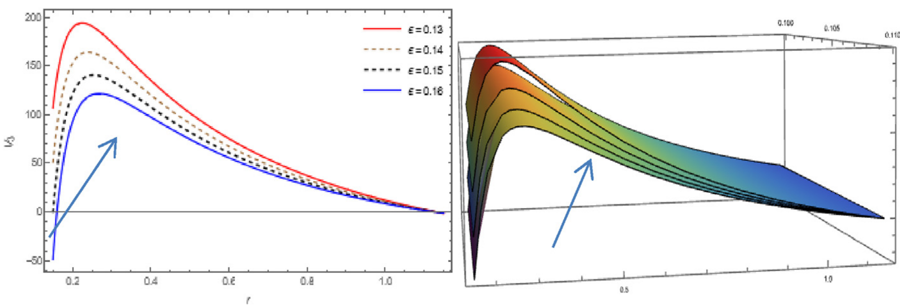

Fig. 14. Velocity distribution for various values of ε *with* $\varnothing = 0.15$, $W_e = 0.03$, $L_5 = 0.1$, $L_4 = 0.5$, $L_3 = 0.1$, $L_1 = 0.1$, $L_2 = 0.1$, $Da = 0.9$, $M = 1.1$, $Gr = 1$, $\Omega = 0.9$, $Pr = 3$, $Rn = 0.5$, $Sr = 0.7$, $Sc = 0.5$, $Gc = 2$, $t = 0.1$, $z = 0.4$.

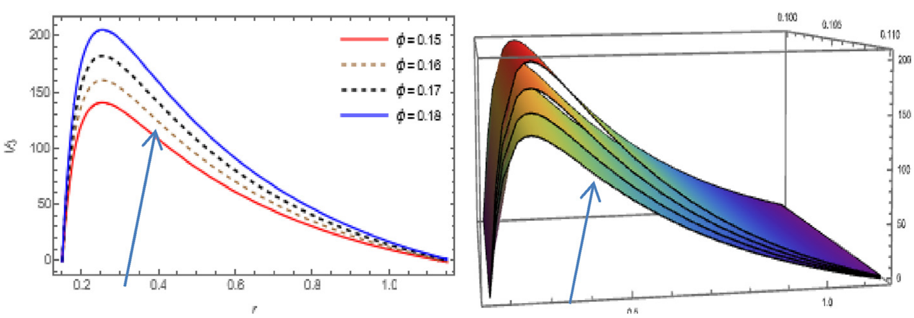

Fig. 15. Velocity distribution for various values of $\varnothing$ *with* $\varepsilon = 0.15$, $W_e = 0.03$, $L_5 = 0.1$, $L_4 = 0.5$, $L_3 = 0.1$, $L_1 = 0.1$, $L_2 = 0.1$, $Da = 0.9$, $M = 1.1$, $Gr = 1$, $\Omega = 0.9$, $Pr = 3$, $Rn = 0.5$, $Sr = 0.7$, $Sc = 0.5$, $Gc = 2$, $t = 0.1$, $z = 0.4$.

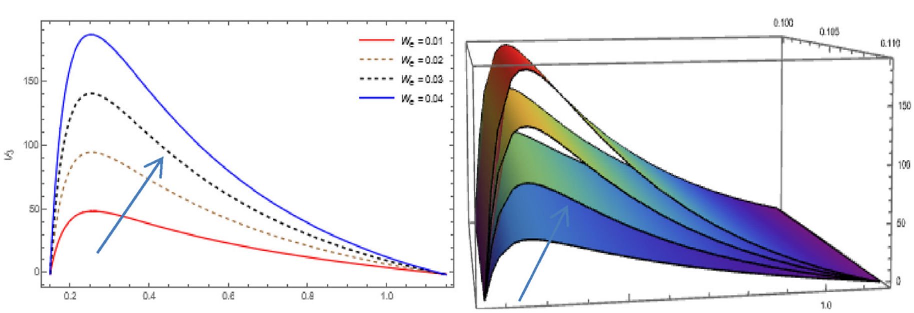

Fig. 16. Velocity distribution for various values of W_e *with* $\varepsilon = 0.15$, $\varnothing = 0.15$, $L_5 = 0.1$, $L_4 = 0.5$, $L_3 = 0.1$, $L_1 = 0.1$, $L_2 = 0.1$, $Da = 0.9$, $M = 1.1$, $Gr = 1$, $\Omega = 0.9$, $Pr = 3$, $Rn = 0.5$, $Sr = 0.7$, $Sc = 0.5$, $Gc = 2$, $t = 0.1$, $z = 0.4$.

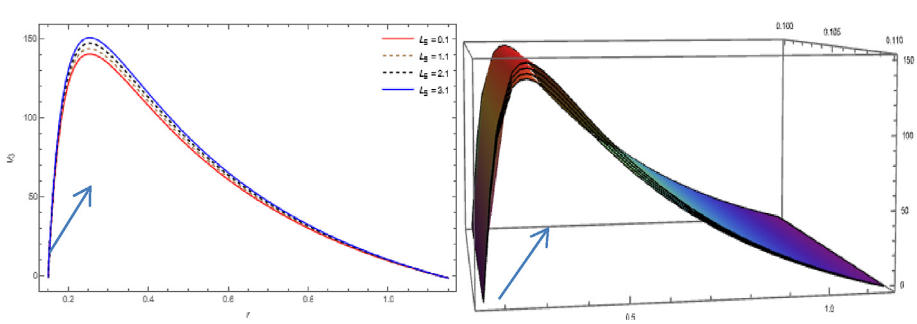

Fig. 17. Velocity distribution for various values of L_5 *with* $\varepsilon = 0.15$, $\varnothing = 0.15$, $W_e = 0.03$, $L_4 = 0.5$, $L_3 = 0.1$, $L_1 = 0.1$, $L_2 = 0.1$, $Da = 0.9$, $M = 1.1$, $Gr = 1$, $\Omega = 0.9$, $Pr = 3$, $Rn = 0.5$, $Sr = 0.7$, $Sc = 0.5$, $Gc = 2$, $t = 0.1$, $z = 0.4$.

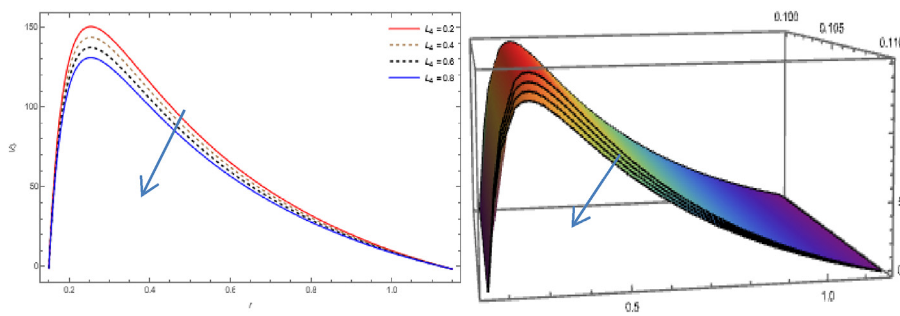

Fig. 18. Velocity distribution for various values of L_4 *with* $\varepsilon = 0.15$, $\varnothing = 0.15$, $W_e = 0.03$, $L_5 = 0.1$, $L_3 = 0.1$, $L_1 = 0.1$, $L_2 = 0.1$, $Da = 0.9$, $M = 1.1$, $Gr = 1$, $\Omega = 0.9$, $Pr = 3$, $Rn = 0.5$, $Sr = 0.7$, $Sc = 0.5$, $Gc = 2$, $t = 0.1$, $z = 0.4$.

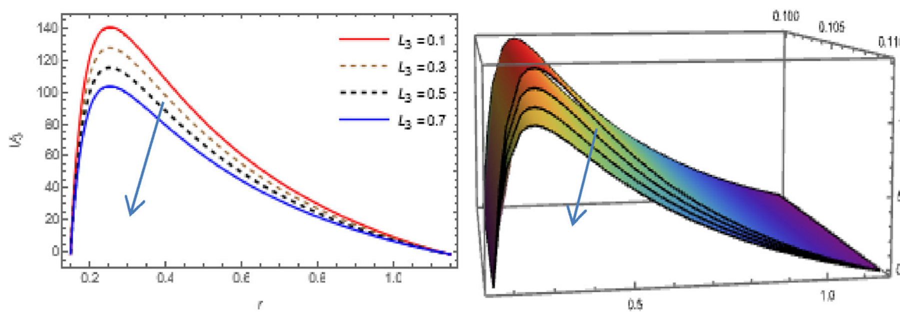

Fig. 19. Velocity distribution for various values of L_3 *with* $\varepsilon = 0.15$, $\varnothing = 0.15$, $W_e = 0.03$, $L_5 = 0.1$, $L_4 = 0.5$, $L_1 = 0.1$, $L_2 = 0.1$, $Da = 0.9$, $M = 1.1$, $Gr = 1$, $\Omega = 0.9$, $Pr = 3$, $Rn = 0.5$, $Sr = 0.7$, $Sc = 0.5$, $Gc = 2$, $t = 0.1$, $z = 0.4$.

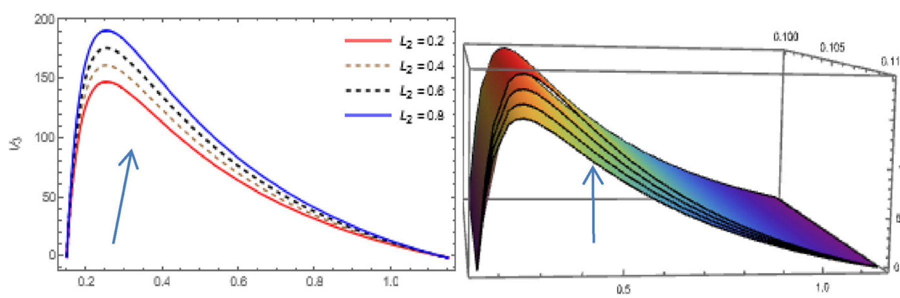

Fig. 20. Velocity distribution for various values of L_2 *with* $\varepsilon = 0.15$, $\varnothing = 0.15$, $W_e = 0.03$, $L_5 = 0.1$, $L_4 = 0.5$, $L_3 = 0.1$, $L_1 = 0.1$, $Da = 0.9$, $M = 1.1$, $Gr = 1$, $\Omega = 0.9$, $Pr = 3$, $Rn = 0.5$, $Sr = 0.7$, $Sc = 0.5$, $Gc = 2$, $t = 0.1$, $z = 0.4$.

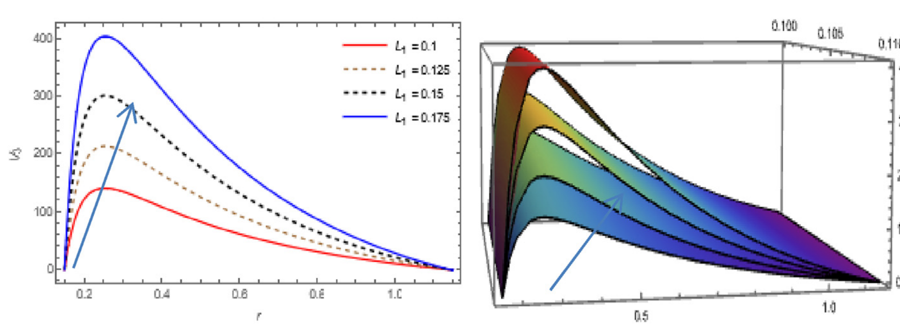

Fig. 21. Velocity distribution for various values of L_1 *with* $\varepsilon = 0.15$, $\varnothing = 0.15$, $W_e = 0.03$, $L_5 = 0.1$, $L_4 = 0.5$, $L_3 = 0.1$, $L_2 = 0.1$, $Da = 0.9$, $M = 1.1$, $Gr = 1$, $\Omega = 0.9$, $Pr = 3$, $Rn = 0.5$, $Sr = 0.7$, $Sc = 0.5$, $Gc = 2$, $t = 0.1$, $z = 0.4$.

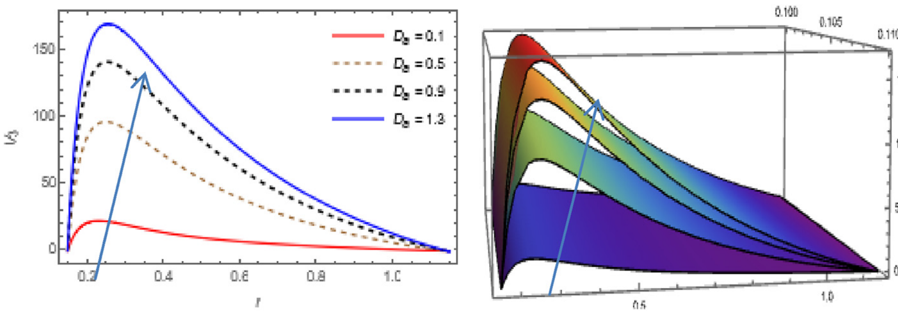

Fig. 22. Velocity distribution for various values of Da with $\varepsilon = 0.15$, $\varnothing = 0.15$, $W_e = 0.03$, $L_5 = 0.1$, $L_4 = 0.5$, $L_3 = 0.1$, $L_1 = 0.1$, $L_2 = 0.1$, $M = 1.1$, $Gr = 1$, $\Omega = 0.9$, $Pr = 3$, $Rn = 0.5$, $Sr = 0.7$, $Sc = 0.5$, $Gc = 2$, $t = 0.1$, $z = 0.4$.

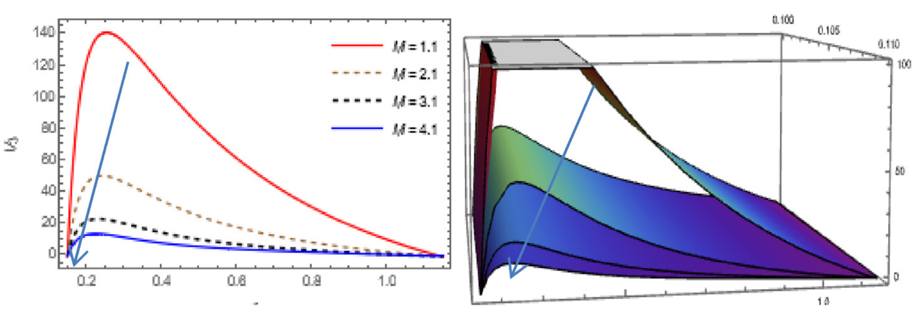

Fig. 23. Velocity distribution for various values of M with $\varepsilon = 0.15$, $\varnothing = 0.15$, $W_e = 0.03$, $L_5 = 0.1$, $L_4 = 0.5$, $L_3 = 0.1$, $L_1 = 0.1$, $L_2 = 0.1$, $Da = 0.9$, $Gr = 1$, $\Omega = 0.9$, $Pr = 3$, $Rn = 0.5$, $Sr = 0.7$, $Sc = 0.5$, $Gc = 2$, $t = 0.1$, $z = 0.4$.

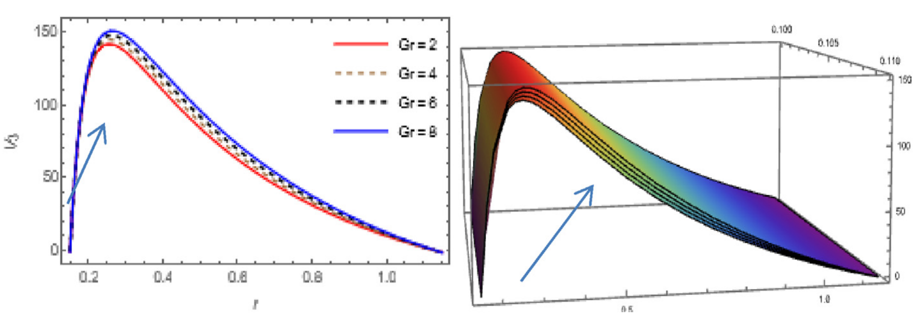

Fig. 24. Velocity distribution for various values of Gr with $\varepsilon = 0.15$, $\varnothing = 0.15$, $W_e = 0.03$, $L_5 = 0.1$, $L_4 = 0.5$, $L_3 = 0.1$, $L_1 = 0.1$, $L_2 = 0.1$, $Da = 0.9$, $M = 1.1$, $\Omega = 0.9$, $Pr = 3$, $Rn = 0.5$, $Sr = 0.7$, $Sc = 0.5$, $Gc = 2$, $t = 0.1$, $z = 0.4$.

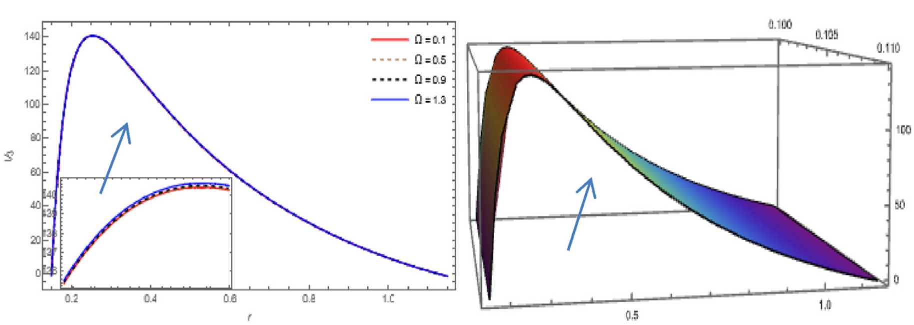

Fig. 25. Velocity distribution for various values of Ω *with* $\varepsilon = 0.15$, $\varnothing = 0.15$, $W_e = 0.03$, $L_5 = 0.1$, $L_4 = 0.5$, $L_3 = 0.1$, $L_1 = 0.1$, $L_2 = 0.1$, $Da = 0.9$, $M = 1.1$, $Gr = 1$, $Pr = 3$, $Rn = 0.5$, $Sr = 0.7$, $Sc = 0.5$, $Gc = 2$, $t = 0.1$, $z = 0.4$.

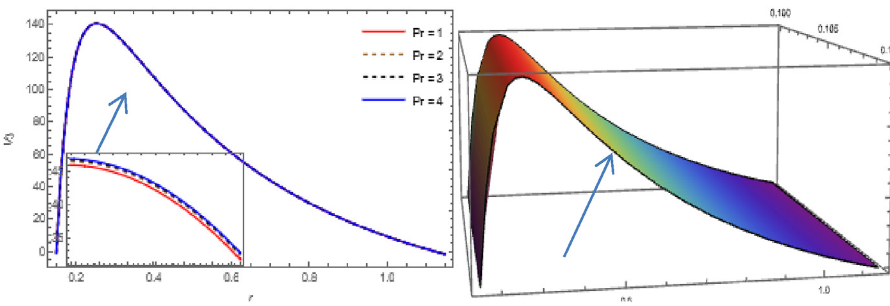

Fig. 26. Velocity distribution for various values of Pr with $\varepsilon = 0.15$, $\varnothing = 0.15$, $W_e = 0.03$, $L_5 = 0.1$, $L_4 = 0.5$, $L_3 = 0.1$, $L_1 = 0.1$, $L_2 = 0.1$, $Da = 0.9$, $M = 1.1$, $Gr = 1$, $\Omega = 0.9$, $Rn = 0.5$, $Sr = 0.7$, $Sc = 0.5$, $Gc = 2$, $t = 0.1$, $z = 0.4$.

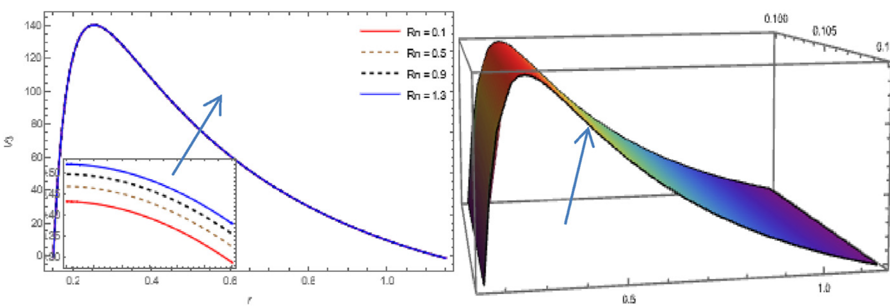

Fig. 27. Velocity distribution for various values of Rn with $\varepsilon = 0.15$, $\varnothing = 0.15$, $W_e = 0.03$, $L_5 = 0.1$, $L_4 = 0.5$, $L_3 = 0.1$, $L_1 = 0.1$, $L_2 = 0.1$, $Da = 0.9$, $M = 1.1$, $Gr = 1$, $\Omega = 0.9$, $Pr = 3$, $Sr = 0.7$, $Sc = 0.5$, $Gc = 2$, $t = 0.1$, $z = 0.4$.

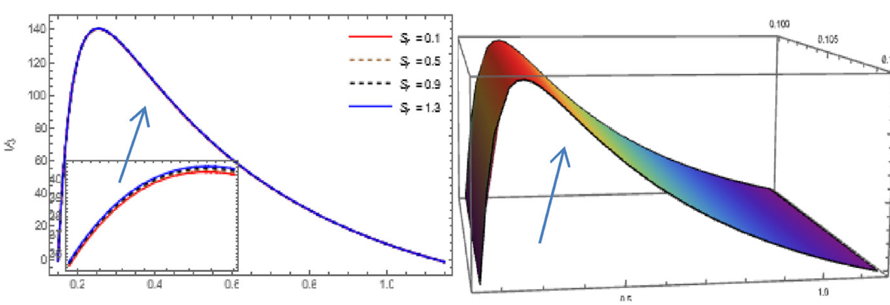

Fig. 28. Velocity distribution for various values of Sr with $\varepsilon = 0.15$, $\varnothing = 0.15$, $W_e = 0.03$, $L_5 = 0.1$, $L_4 = 0.5$, $L_3 = 0.1$, $L_1 = 0.1$, $L_2 = 0.1$, $Da = 0.9$, $M = 1.1$, $Gr = 1$, $\Omega = 0.9$, $Pr = 3$, $Rn = 0.5$, $Sc = 0.5$, $Gc = 2$, $t = 0.1$, $z = 0.4$.

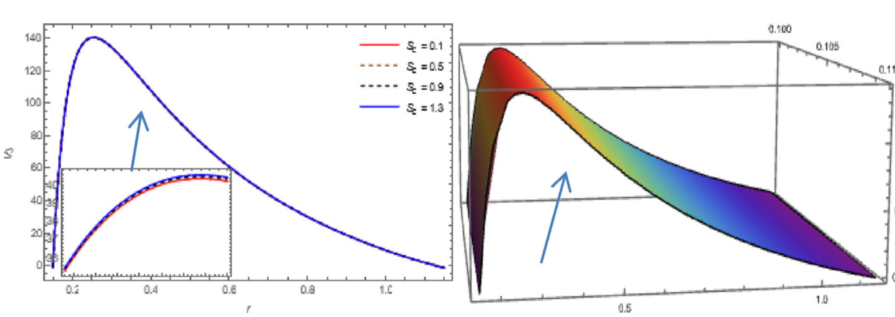

Fig. 29. Velocity distribution for various values of Sc with $\varepsilon = 0.15$, $\varnothing = 0.15$, $W_e = 0.03$, $L_5 = 0.1$, $L_4 = 0.5$, $L_3 = 0.1$, $L_1 = 0.1$, $L_2 = 0.1$, $Da = 0.9$, $M = 1.1$, $Gr = 1$, $\Omega = 0.9$, $Pr = 3$, $Rn = 0.5$, $Sr = 0.7$, $Gc = 2$, $t = 0.1$, $z = 0.4$.

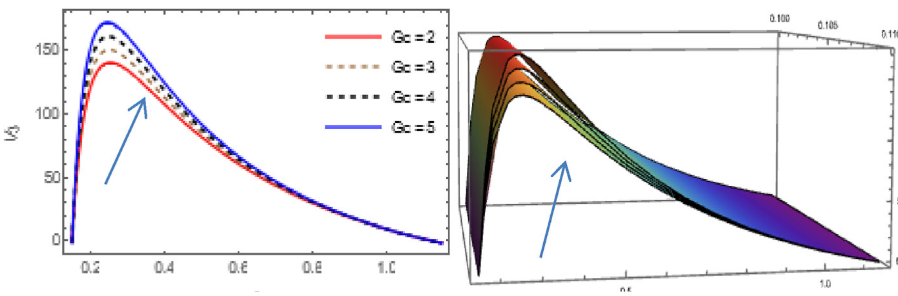

Fig. 30. Velocity distribution for various values of Gc with $\varepsilon = 0.15$, $\varnothing = 0.15$, $W_e = 0.03$, $L_5 = 0.1$, $L_4 = 0.5$, $L_3 = 0.1$, $L_1 = 0.1$, $L_2 = 0.1$, $Da = 0.9$, $M = 1.1$, $Gr = 1$, $\Omega = 0.9$, $Pr = 3$, $Rn = 0.5$, $Sr = 0.7$, $Sc = 0.5$, $t = 0.1$, $z = 0.4$.

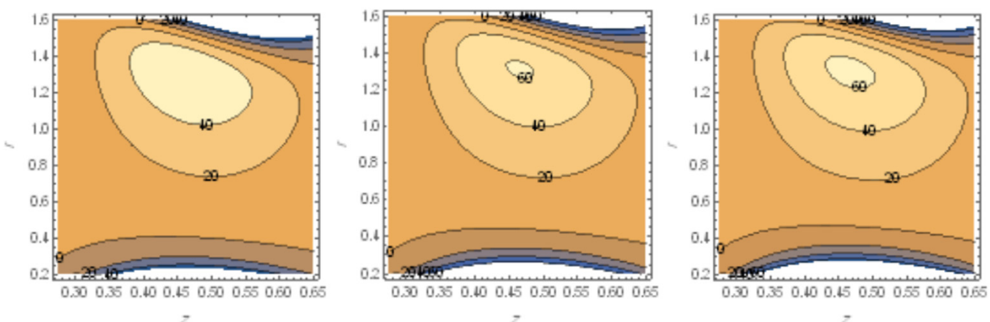

Fig. 31. Wave frame streamlines for different values of $\varepsilon = \{0.15, 0.2, 0.225\}$ *at* $\varnothing = 0.15$, $W_e = 0.03$, $L_5 = 0.1$, $L_4 = 0.5$, $L_3 = 0.1$, $L_1 = 0.1$, $L_2 = 0.1$, $Da = 0.9$, $M = 1.1$, $Gr = 1$, $\Omega = 0.9$, $Pr = 3$, $Rn = 0.5$, $Sr = 0.7$, $Sc = 0.5$, $Gc = 2$, $t = 0$.

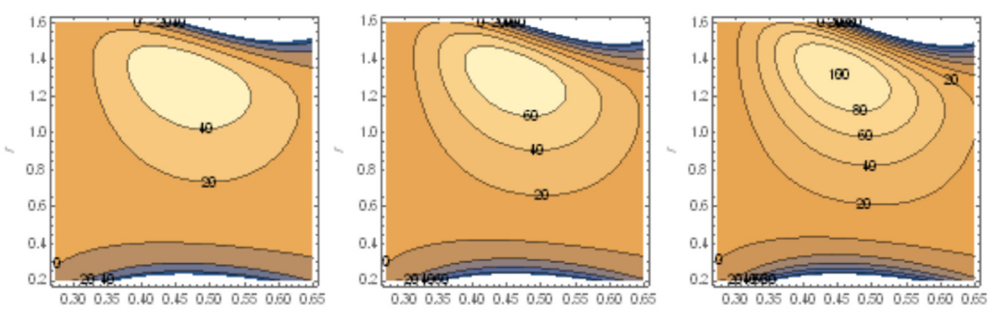

Fig. 32. Wave frame streamlines for different values of $\phi = \{0.15, 0.175, 0.2\}$ *at* $\varepsilon = 0.15$, $W_e = 0.03$, $L_5 = 0.1$, $L_4 = 0.5$, $L_3 = 0.1$, $L_1 = 0.1$, $L_2 = 0.1$, $Da = 0.9$, $M = 1.1$, $Gr = 1$, $\Omega = 0.9$, $Pr = 3$, $Rn = 0.5$, $Sr = 0.7$, $Sc = 0.5$, $Gc = 2$, $t = 0$.

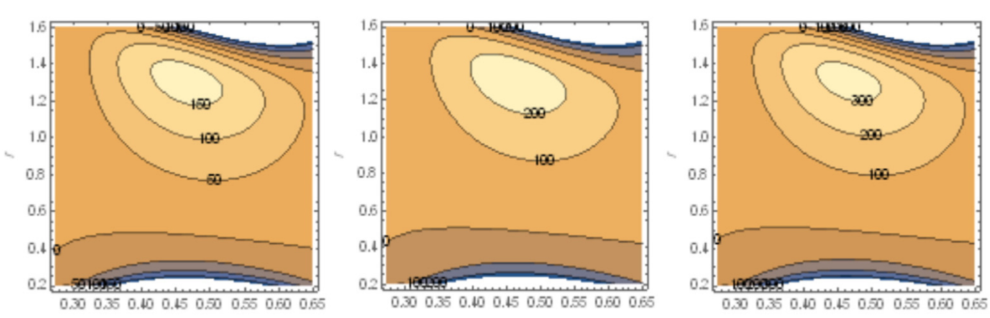

Fig. 33. Wave frame streamlines for different values of $W_e = \{0.1, 0.15, 0.2\}$ *at* $\varepsilon = 0.15$, $\varnothing = 0.15$, $L_5 = 0.1$, $L_4 = 0.5$, $L_3 = 0.1$, $L_1 = 0.1$, $L_2 = 0.1$, $Da = 0.9$, $M = 1.1$, $Gr = 1$, $\Omega = 0.9$, $Pr = 3$, $Rn = 0.5$, $Sr = 0.7$, $Sc = 0.5$, $Gc = 2$, $t = 0$.

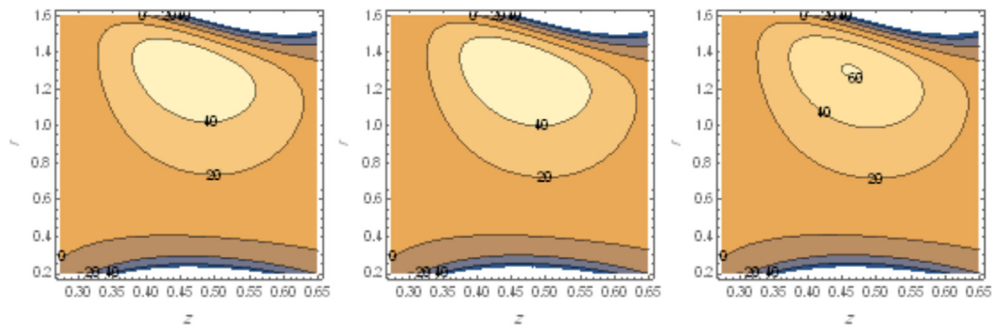

Fig. 34. Wave frame streamlines for different values of $L_5 = \{0.1, 2.1, 3.1\}$ *at* $\varepsilon = 0.15$, $\varnothing = 0.15$, $W_e = 0.03$, $L_4 = 0.5$, $L_3 = 0.1$, $L_1 = 0.1$, $L_2 = 0.1$, $Da = 0.9$, $M = 1.1$, $Gr = 1$, $\Omega = 0.9$, $Pr = 3$, $Rn = 0.5$, $Sr = 0.7$, $Sc = 0.5$, $Gc = 2$, $t = 0$.

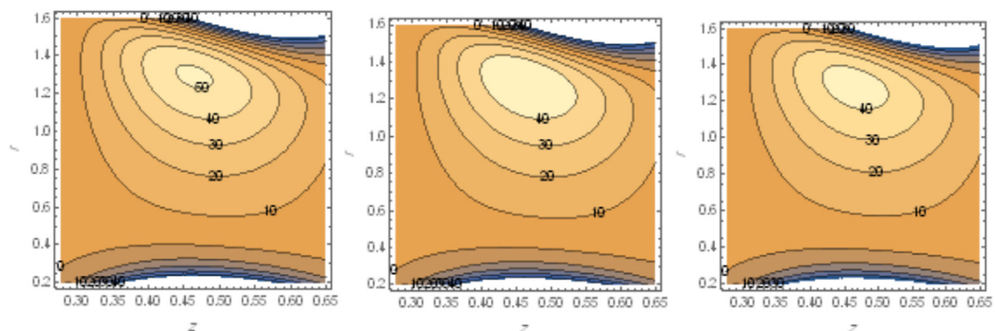

Fig. 35. Wave frame streamlines for different values of $L_3 = \{0.3, 0.4, 0.6\}$ *at* $\varepsilon = 0.15$, $\varnothing = 0.15$, $W_e = 0.03$, $L_5 = 0.1$, $L_4 = 0.5$, $L_1 = 0.1$, $L_2 = 0.1$, $Da = 0.9$, $M = 1.1$, $Gr = 1$, $\Omega = 0.9$, $Pr = 3$, $Rn = 0.5$, $Sr = 0.7$, $Sc = 0.5$, $Gc = 2$, $t = 0$.

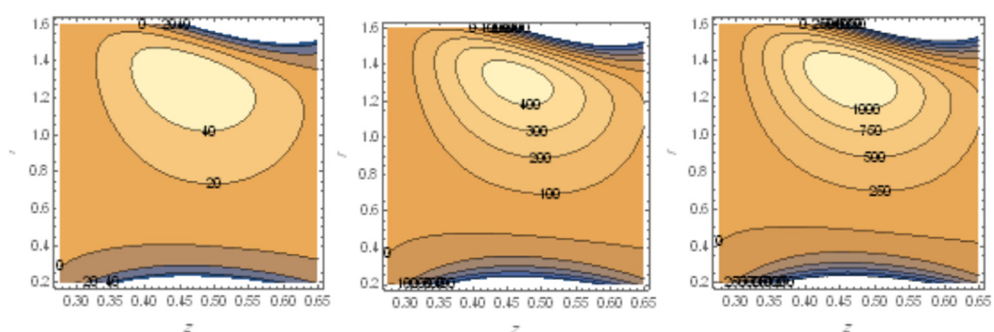

Fig. 36. Wave frame streamlines for different values of $L_1 = \{0.1, 0.3, 0.5\}$ *at* $\varepsilon = 0.15$, $\varnothing = 0.15$, $W_e = 0.03$, $L_5 = 0.1$, $L_4 = 0.5$, $L_3 = 0.1$, $L_2 = 0.1$, $Da = 0.9$, $M = 1.1$, $Gr = 1$, $\Omega = 0.9$, $Pr = 3$, $Rn = 0.5$, $Sr = 0.7$, $Sc = 0.5$, $Gc = 2$, $t = 0$.

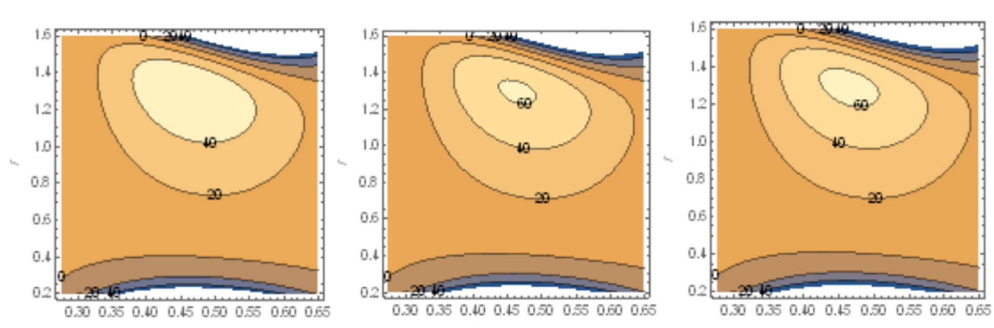

Fig. 37. Wave frame streamlines for different values of $L_2 = \{0.1, 0.3, 0.4\}$ *at* $\varepsilon = 0.15$, $\varnothing = 0.15$, $W_e = 0.03$, $L_5 = 0.1$, $L_4 = 0.5$, $L_3 = 0.1$, $L_1 = 0.1$, $Da = 0.9$, $M = 1.1$, $Gr = 1$, $\Omega = 0.9$, $Pr = 3$, $Rn = 0.5$, $Sr = 0.7$, $Sc = 0.5$, $Gc = 2$, $t = 0$.

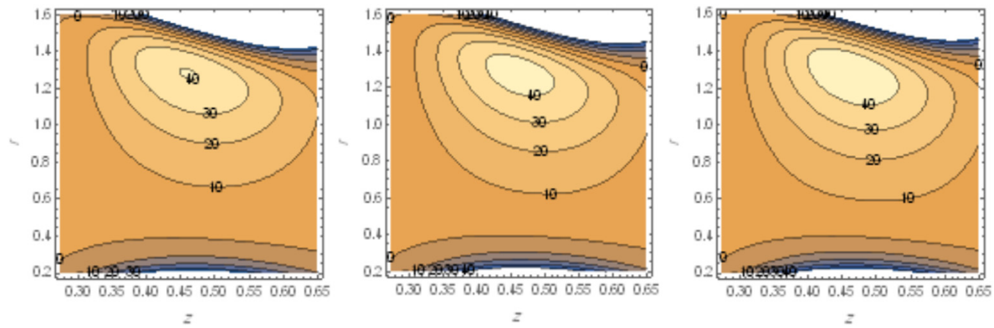

Fig. 38. Wave frame streamlines for different values of $Da = \{0.4, 0.5, 0.6\}$ *at* $\varepsilon = 0.15$, $\varnothing = 0.15$, $W_e = 0.03$, $L_5 = 0.1$, $L_4 = 0.5$, $L_3 = 0.1$, $L_1 = 0.1$, $L_2 = 0.1$, $M = 1.1$, $Gr = 1$, $\Omega = 0.9$, $Pr = 3$, $Rn = 0.5$, $Sr = 0.7$, $Sc = 0.5$, $Gc = 2$, $t = 0$.

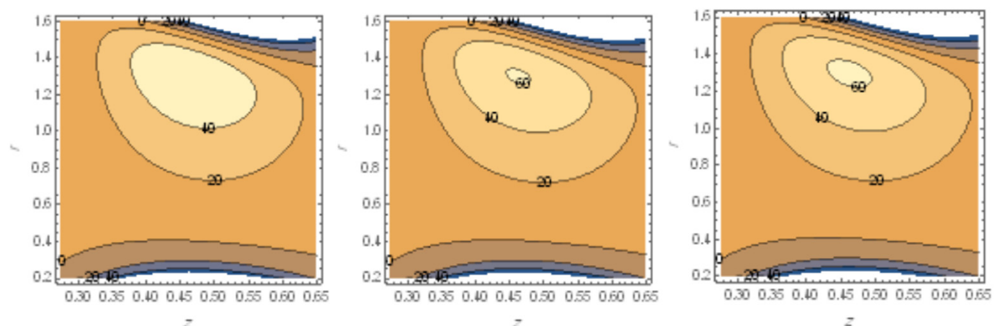

Fig. 39. Wave frame streamlines for different values of $Gr = \{2, 6, 8\}$ *at* $\varepsilon = 0.15$, $\varnothing = 0.15$, $W_e = 0.03$, $L_5 = 0.1$, $L_4 = 0.5$, $L_3 = 0.1$, $L_1 = 0.1$, $L_2 = 0.1$, $Da = 0.9$, $M = 1.1$, $Gr = 1$, $\Omega = 0.9$, $Pr = 3$, $Rn = 0.5$, $Sr = 0.7$, $Sc = 0.5$, $Gc = 2$, $t = 0$.

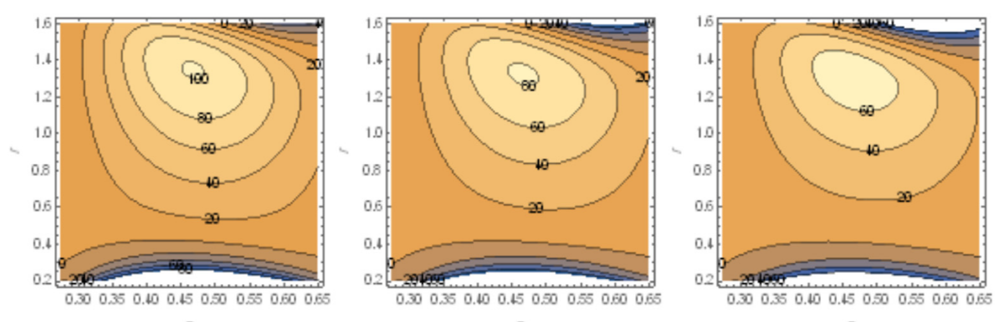

Fig. 40. Wave frame streamlines for different values of $M = \{0.2, 0.6, 0.8\}$ *at* $\varepsilon = 0.15$, $\varnothing = 0.15$, $W_e = 0.03$, $L_5 = 0.1$, $L_4 = 0.5$, $L_3 = 0.1$, $L_1 = 0.1$, $L_2 = 0.1$, $Da = 0.9$, $Gr = 1$, $\Omega = 0.9$, $Pr = 3$, $Rn = 0.5$, $Sr = 0.7$, $Sc = 0.5$, $Gc = 2$, $t = 0$.

7. Concluding remarks

Studying the influence of wall characteristics on the peristaltic flow of incompressible Williamson fluid led to significant findings. Turbulence theory was used to address the issue, and the program MATHEMATICA was used to discuss how parameters affected fluid movement by examining the resulting graphs.

- The temperature is decreasing with increasing ε, R_n, Ω and Pr while increasing with increase $\varnothing$.
- The Concentration has a direct effect on parameters ε, R_n, Ω , $\varnothing$, Sr, Sc and Pr .
- The velocity of fluid increases by increasing of $\varnothing$, W_e, L_5, L_2, L_1, Rn, Sr, Sc, Pr, Gc, D_a, Gr, and Ω while The velocity of fluid decreasing with increasing ε, L_3, L_4 and M.
- The trapped bolus increases with the increasing $\varnothing$, W_e, L_5, L_2, L_1, D_a, and Gr, while The trapped bolus of fluid decreasing with increasing L_3 and M.

Funding

Self-funding.

References

[1] Kotnurkar AS, Kallolikar N. Influence of metachronal ciliary wave motion on peristaltic flow of nanofluid model of synovitis problem. AIP Adv 2022;12(5):55217.
[2] Gajbhare BP, Krishnaprasad J, Mishra S. Peristaltic flow of Buongiorno model nanofluids within a sinusoidal wall surface used in drug delivery. Heat Transf 2020;49(2):1016−34.
[3] Latham TW. Fluid motions in a peristaltic pump. Massachusetts Institute of Technology; 1966.
[4] Shapiro AH, Jaffrin MY, Weinberg SL. Peristaltic pumping with long wavelengths at low Reynolds number. J Fluid Mech 1969;37(4):799−825.
[5] Sunitha G. Influence of thermal radiation on peristaltic blood flow of a Jeffrey fluid with double diffusion in the presence of gold nanoparticles. Inform Med Unlocked 2019;17:100272.
[6] Al-Aridhee AAH, Al-Khafajy DGS. Influence of MHD peristaltic transport for jeffrey fluid with varying temperature and concentration through porous medium. J Phys Conf 2019;1294(3):32012.
[7] AL-khulaifawi SFJ, Al-Khafajy DGS. MHD peristaltic flow of a couple-stress with varying temperature for jeffrey fluid through porous medium. J Phys Conf 2020;1591(1): 12075.
[8] Riaz A, Zeeshan A, Ahmad S, Razaq A, Zubair M. Effects of external magnetic field on non-Newtonian two phase fluid in an annulus with peristaltic pumping. Jpn Mag 2019;24(1): 62−9.
[9] Al-Khafajy DGS, Abd Alhadi A. Magnetohydrodynamic Peristaltic flow of a couple stress with heat and mass transfer of a Jeffery fluid in a tube through porous medium. Adv Phys Theor Appl 2014;32:638−2225.
[10] Naz R, Noor M, Shah Z, Sohail M, Kumam P, Thounthong P. Entropy generation optimization in MHD pseudoplastic fluid comprising motile microorganisms with stratification effect. Alex Eng J 2020;59(1):485−96.